Chapter 2

ATMOSPHERIC INPUT OF MANGANESE AND IRON TO THE OCEAN:

Seawater dissolution experiments with Saharan and North American dusts

Jeffrey Mendez[a], Cecile Guieu[b1], Jess Adkins[b]

[a] Department of Environmental Science and Engineering, California Institute of Technology
[b] Department of Geological and Planetary Sciences, California Institute of Technology

Abstract

Dissolution of wind blown dust is a major source of iron, manganese, and other trace nutrients in the ocean. Kinetic and thermodynamic values for the release of metals from dust are needed for computer models which incorporate dust as part of their ocean system. Here we investigate both the thermodynamic and kinetics parameters involved in the dissolution of metals from dust in seawater. We added dust from the Sahara and the Western United States in five different concentrations (0.01 - 5.0 mg/L), representative of those concentrations found in seawater after dust events, to open ocean Pacific seawater. Sub-sampling of the reaction vessels took place on days 1, 2, 4, 7, 14, and 35 for the kinetic study.

Results show different apparent thermodynamic constants for manganese (Mn) and iron (Fe). The final Mn concentrations are proportional to the added dust concentration. Fe concentrations reach a maximum of less than 2 nM, independent of the quantity and type of dust added. The Fe dissolution kinetics are faster than our sampling resolution. The first order rate constant for the dissolution of Mn from the Western US and Sahara dusts were $0.94 \pm 0.04 \, \frac{nmol \, \text{Mn}}{day \cdot mg \, \text{Dust}}$ and $0.22 \pm 0.01 \, \frac{nmol \, \text{Mn}}{day \cdot mg \, \text{Dust}}$, respectively. We conclude

[1] Now at: Université Pierre et Marie Curie-Paris, CNRS, Laboratoire d'Océanographie de Villefranche (LOV), 06238 Villefranche-sur-mer, France, France, guieu@obs-vlfr.fr

that Mn concentrations are limited by available Mn on the dust surface, while Fe concentrations are limited by the ligand concentrations in the seawater, which ultimately are determined by the biological community.

1. Introduction

1.1 Dust as a Metal Source

Windblown dust is an important source of many trace metals to the open ocean. Metals such as aluminum (Al) (Measures *et al.*, 1986) and lead (Pb) (Nozaki *et al.*, 1980) have a typical atmospheric deposition profile with high concentrations in the surface due to contact with the atmosphere and a sharp decrease with depth. Manganese (Mn) (Klinkhammer and Bender, 1980) and iron (Fe) (Martin and Fitzwater, 1988) have more complicated profiles and are nutrients for phytoplankton in the ocean. Although there are many sources of Mn and Fe to the ocean, wind blown dust is the largest source to the open ocean (Duce and Tindale, 1991; Guieu et al., 1994). The degree to which eolian Fe and Mn dissolve and are accessible to the phytoplankton community is the focus of this study.

1.2 Iron

Although Fe is the fourth most abundant element in the Earth's crust, dissolved Fe concentrations in open-ocean seawater are extremely low. Dissolved Fe in the +3 oxidation state, the redox species believed to dominate in oxygenated seawater, has very low solubility with respect to Fe(III) oxyhydroxide solids (Morel and Herring, 1993). Above this solubility limit Fe is kept in the dissolved form with organic ligands (Barbeau *et al.*, 2001; Buck, 2007; Küpper *et al.*, 2006; Rue and Bruland, 1995; van den Berg, 1995). These ligands, produced by bacteria and phytoplankton, keep Fe in solution and available for biological uptake (Barbeau, 2006; Haygood *et al.*, 1993; Kraemer *et al.*, 2005).

Bottle incubations and mesoscale Fe addition experiments have shown Fe to be important to ocean productivity, and in many locations, the limiting or co-limiting nutrient. Computer models have incorporated Fe (Aumont *et al.*, 2003; Moore *et al.*, 2006) to more accurately

describe ocean biogeochemical cycles. Dust is the major source of Fe to the open ocean that cannot be reached by river deposits. Unfortunately, the amount and mechanism of Fe release from dust is not well understood. Recent models have used a wide range of Fe solubilities, ranging from 1-10% of the total Fe in the dust. In addition, there have been variations in the estimates of total dust deposition itself, based on measurements (Duce and Tindale, 1991; Gao *et al.*, 2003), modeling results (Tegen and Fung, 1994), and the speciation of the iron within the deposited dust (Hand *et al.*, 2004). To more accurately represent Fe within these models, more needs to be known about the exact nature of Fe dissolution from dust.

1.3 Manganese

Manganese is an important micronutrient for marine organisms via its use in photosynthetic and radical scavenging enzymes (Horsburgh *et al.*, 2002; Kernen *et al.*, 2002). Thermodynamically, an oxygenated ocean at a pH of 8 should lead to the insoluble Mn(IV) species in the form MnO_2. Dissolved Mn ocean profiles reveal that the surface waters contain high levels of soluble Mn(II). A portion of the soluble Mn is from direct atmospheric deposition, which contains Mn in the +2 oxidation state (Guieu et al., 1994; Siefert et al., 1998). Slow oxidation to the +3 or +4 state allows Mn to stay dissolved on the order of days. However, Mn still should oxidize over time and precipitate out of the surface ocean (Stumm and Morgan, 1996). This oxidation is prevented by photoreduction of Mn to the soluble +2 state in the presence of organic material (Sunda *et al.*, 1983), resulting in a large concentration of Mn in the surface water available for biological use.

1.4 Dust Experiments

Past dust dissolution experiments in seawater (Bonnet and Guieu, 2004; Buck *et al.*, 2006) have sought to address the question of how dust affects the Fe concentration of the surface ocean. Bonnet and Guieu, (2004) allowed ocean water to sit with different concentrations of Saharan dust for 24 hours and 7 days. Their experiment provided information on the thermodynamics of Fe dissolution revealing that 0.55 to 2.2% of the soil's Fe made its way

into the dissolved form. This result is on the low end of previous assumptions. Experiments conducted by Buck et. al., 2006 describe a different type of solubility, in which aerosols collected by air filtration were briefly exposed to seawater. This type of experiment measures the instantaneous dissolution or the leachable Fe component from the aerosols. Buck et. al., 2006 found that 6 ± 5 % of the Fe was leached from the aerosol particles in seawater. Yet there are still many questions about the mechanism and extent of dust dissolution, and the Fe solubility from this dust. Is instantaneous dissolution relevant to an element which is insoluble and highly reactive with OH^- and O_2, or is it in fact more relevant to measure the instantaneous dissolution because Fe may be precipitated quickly? In addition, what is the behavior of different types of mineral dusts and different dust concentrations in seawater? Our experiment has attempted to address these last two questions by conducting various bottle experiments using two different dust samples over a wide range of dust concentrations, and taking sub-samples over time to measure the dissolution progress and the initial rate constants.

2. Method

2.1 Collection and Experimental Set-up

Seawater was collected at 30°N 140°W in November 2004, aboard the RV Melville using the UC Santa Cruz trace metal surface sampler. This seawater was inline filtered at 0.2 μm (Pall #12941) into an acid leached 25 L polyethylene carboy and later stored in the dark.

Saharan dust is a composite of 12 surface soils that were collected under clean conditions from the Hoggar region (Algeria). U.S. dust is a composite of 3 superficial deposits collected in natural dust traps in the Nevada desert (South-West of Las Vegas). Both Saharan and U.S. dust have been hand sieved through successive clean polyethylene meshes of 100 and 20 μm pore diameter. The smallest fraction (<20 μm) was collected and stored in a clean glass bottle. The U.S. sample was then autoclaved to destroy any possible bacteria spores, and both samples were stored in a dark cabinet.

Samples were prepared by adding seawater to five 1 L clear Teflon bottles using an acid leached graduated cylinder. In a 1 L polyethylene bottle, 10 mg of Saharan dust was added to 1 L of seawater. This solution was quickly shaken and proportioned via pipette or graduated cylinder to each of the sample bottles in order to reach the different dust concentrations (0.01, 0.05, 0.5, 1.0, 5.0 mg/L). The sample bottles (including a control bottle which received no dust) were then sealed with parafilm and immersed in a 13°C water bath (temperature of nitracline), under a 50% light screen (to mimic the reduced light in the euphotic zone), on the roof of the laboratory. This sequence was repeated for the U.S. dust. The seawater was allowed to mature under the diurnal cycle for 35 days. Samples were removed from this bath on days 1, 2, 4, 7, 14, and 35 at 1:00 PM. Sub-sampling lasted for ~2 hours, and then the reservoir was returned to the water bath on the roof.

Sub-samples were taken to measure the progression of metal dissolution. Once removed from the roof, the bottles' exteriors were cleaned by thoroughly rinsing with mQ water in a class 100 laminar flow bench. The parafilm was removed, and the bottles were individually opened for sub-sampling. The filter apparatus was rinsed by pouring 10 mL of the sample through a 25 mm Whatman 0.2 μm polycarbonate membrane filter (Cat #110606). The sub-sample was then taken by pouring another 10 mL of sample through the filter and collecting it in a small high density polyethylene bottle. This sub-sample was immediately split into two and acidified with 10 mL of concentrated (12 M) SeaStar® hydrochloric acid (HCl). Following each sample, the filter was exchanged and the filter apparatus was rinsed with dilute nitric acid (~25 mL SeaStar® 5% (by volume) HNO_3), followed by clean milli-Q water (~150 mL).

2.2 Laboratory Procedures

All sample preparations were conducted within a Class 100 laminar flow bench using trace metal clean techniques. Seawater samples were processed using a modified Isotope

Dilution MagIC (**Mag**nesium **I**nduced **C**o-precipitation) method (Wu and Boyle, 1997; Wu and Boyle, 1998), amplifying the reactive metal concentrations by a factor of 20.

Because it is monoisotopic, Mn was measured using a modified isotope dilution method. Mn concentrations were measured using both an internal ^{57}Fe isotope spike and an external standard calibration line between ^{55}Mn and the ^{57}Fe spike. The internal ^{57}Fe spike set the initial elemental ratio between Fe and Mn and reduced the effects of sensitivity fluctuations during analysis. The external standardization provided a calibration for differences between Fe and Mn during the chemical processing and analysis. These external Mn standards (ranging from 0.5 nM to 10 nM) were prepared by adding small volumes of a $MnNO_3$ solution to 1 mL of low manganese seawater. An ^{57}Fe spike equivalent to the total dissolved Mn concentration in the samples was added to the Mn standards and taken through the modified MagIC procedure.

The metal blank associated with chemical handling was determined by processing 50 μL of "blank" seawater (which has been determined to have 0.65 nM Mn and 0.07 nM Fe) through MagIC, similar to Wu and Boyle's blank analysis. Spiking and precipitation of the blanks are similar to the samples, except it was necessary to add 4-5 times the volume of ammonium hydroxide because the smaller quantity of initial Mg was more difficult to precipitate.

Mass fractionation in the sample uptake and delivery system was corrected by running spiked gravimetric standards (SGSs), which have a known isotopic ratio near the value of our spiked samples. SGS are measured using the same mass spectrometer method, and the measured, mass fractionated, SGS isotope ratio is corrected back to the known isotope ratio. That correction factor can then be used on all samples run during that analysis. SGS were prepared by adding 25 μL of a concentrated SGS solution to 1 mL of the "blank" seawater and then taking the mixture through the MagIC chemistry. This results in a SGS sample with the same solution matrix as our samples and a total Fe concentration of 22 nM.

2.3 Sample Analysis

All samples, standards, and chemical blanks were analyzed in an identical manner on a Finnigan Element I magnetic sector Inductively Coupled Plasma Mass Spectrometer (ICP-MS). Analysis of Fe and Mn was conducted in medium resolution to separate the natural isotopes from argon interferences (^{55}Mn and ^{40}Ar^{15}N, ^{56}Fe and ^{40}Ar^{16}O, ^{57}Fe and ^{40}Ar^{16}O^{1}H). The machine blank was measured by analyzing dilute HNO$_3$ through the same analysis method and subtracting it from the samples before evaluating the ratio. This number was regularly less than 2% of the Mn and Fe signals.

The measured ratios of each SGS were adjusted to the known "true" ratio using a linear fractionation law. Sample ratios were then multiplied by the SGS correction factor (changes varied by 28.5 ± 14.6 ‰/Δamu per run) to yield final ratios of the spike sample. Each sample's [Fe] was determined by using the isotope dilution equation:

$$C_{sa} = \frac{\left(R_{sp} - R_m\right)}{\left(R_m - R_{sa}\right)} \frac{V_{sp}}{V_{sa}} \frac{\%^{57}Fe_{sp}}{\%^{57}Fe_{sa}} C_{sp} \quad , \qquad \text{(eq. 1)}$$

where C is the concentration, R is the isotope ratio, V is volume, and the subscripts sa, sp, and m represent sample, spike, and measured, respectively. The unspiked sample isotope ratio is assumed to be the natural iron isotope ratio (^{56}Fe/^{57}Fe = 43.3006). Uncertainties in the calculated sample concentration were determined from the standard error of the mean of R_m. This number was estimated from multiple scans of the isotope ratio (n= 17 to 40) and matches the external reproducibility of replicates from the same water. Preliminary sample concentrations of Mn were calculated using the elemental ratio of:

$$\left(\frac{^{55}Mn}{^{57}Fe}\right)_m = \frac{Mn}{\left(^{57}Fe_{sp} + ^{57}Fe_{sa}\right)} \quad . \qquad \text{(eq. 2)}$$

These concentrations were divided by the slope of the standard calibration line to correct for efficiency differences between Mn and Fe in the chemical and ICP-MS process. This accounted for a 10-20% decrease depending on the day of processing and analysis.

Dust was acid digested inside a Milestone 1200 Mega microwave oven with 1 mL of HF (concentrated Suprapur®, Merck, 40% in volume, in polypropylene container) and 3 mL HNO$_3$ (concentrated Suprapur®, Merck, 65% v/v). Aluminum (Al), Fe, and Mn were determined using calibration curves by Inductively Coupled Plasma-Atomic Emission Spectroscopy (ICP-AES 'Ultra traces', Jobin Yvon). Blanks (reagent alone) were below the detection limit. The ratio of measured-to-recommended concentrations in the BCSS certified reference material ((n=3), National Research Council of Canada; range of weights: 10.7-16.08 mg) was Fe = 1.06 ± 0.05, Al = 0.99 ± 0.05, Mn = 1.05 ± 0.04. Grain-size distributions in volume were established for the two dust samples dispersed in ultrapure water with a Mastersizer (Malvern Instruments, UK).

3. Results

3.1 Seawater sub-samples

Figure 1 shows dissolved (a) Mn and (b) Fe concentration versus time after dust addition. In general, dissolved Fe concentrations increase to about 0.5 nM by the first sub-sample and slowly increase to 1-1.5 nM over the course of the experiment. Dissolved Mn increases in proportion to dust concentration, with dust from the United States releasing Mn faster than dust from the Sahara.

3.2 Dust

Elemental analysis of the dusts used in our experiment show Mn, Fe, and Al concentrations similar to crustal abundances (Table 1). The grain size distributions measured in percentage of total volume per grain size are plotted in figure 2. The Saharan dust volume is shifted to smaller grain sizes compared to the U.S. dust. These distributions are in good agreement with the size spectrum obtained on Saharan end-member transported dust whose median

size was ~8 μm (this is the average size distribution of the particulate phase of six Saharan rains collected in Corsica and selected among a 12 year series to be as representative as possible of pure Saharan end-member, see details in (Guieu *et al.*, 2002,) indicating that the <20 μm fraction of the Saharan and U.S. soils are a suitable representation of an aeolian component that can be transported over short and medium range distance (like it is the case in the Mediterranean Sea) and possibly long distance.

3.3 Data Quality

  Replicate analyses in the dissolution experiment are generally consistent, but Fe duplicates are less consistent than Mn duplicates due to their higher susceptibility to contamination. The laboratory seawater consistency standards processed and analyzed along with the sub-samples had measured Fe concentrations of 0.042 ± 0.030 nM, n=11, which is in agreement with all other previous analysis of this standard, [Fe] 0.05 ± 0.03 nM, n=28. Because the precision in these standards is high (measured within 30 pM of each other), we believe that variability between duplicates is a function of sample collection rather than chemical processing or analysis. Accuracy was checked by repeated measurement of three archived samples originally collected and measured by Sophie Bonnet (collection and measurement methods can be found in (Bonnet and Guieu, 2004)). The concentration of these samples (Fe concentrations of 1.37 nM, 0.83 nM, 0.89 nM) were found to be within ±0.03 nM of the previous measurements. Measurements of Mn in the consistency standard are 0.65 ± 0.03 nM, n=11 during this dissolution experiment, which is in agreement with all previous measurements (0.66 ± 0.06 nM, n=28).

Sub-samples collected on day 2 were subject to an unknown source of contamination leading to 40% of all samples taken on that day being over 25 nM for Fe and 30 nM for Mn, many of which were an unrealistic 100 - 5000 nM. All data from day 2 have been discarded. Other sub-samples not represented in the graphs are off scale and believed to be contaminated (control=1, U.S. dust = 1, Saharan dust = 2).

4. Discussion

4.1 Manganese

4.1.1 Mn Kinetics

All raw Mn data is shown in figure 1a. The dissolution rate of Mn (and Fe) is defined by the total increase in metal concentration over time. In order to highlight the different dissolution rates of the dusts, we plot the 5 mg/L data, which has the largest increase in dissolved Mn, in figure 3. The U.S. dust releases Mn into solution faster than the Saharan dust. After this initial increase, the dissolution slows and the [Mn] approaches a plateau after 14-21 days. To measure the initial rate of Mn dissolution, a best straight line fit over the initial linear portion of the curve was performed. The rapid dissolution in the 1 and 5 mg/L U.S. dust samples was a limit in defining this line to only the first two points (days 0-1). The Mn increase is slower in the U.S. samples containing less dust and all the Saharan samples, and we are able to incorporate days 0-4 in the line fits.

We plot the initial slopes versus their corresponding dust concentration in figure 4. The linear trend in the data indicates a first order reaction with dust; therefore, we can write a simple kinetic reaction, equation 3,

$$\frac{d\,\mathrm{Mn}}{dt} = k[Dust] \quad . \qquad\qquad (\text{eq. 3})$$

Error associated with each point in this graph is the error associated with uncertainty in the slope calculation. The 1 and 5 mg/L U.S. dust samples have the largest error because only two points could be used. Manganese in the 0.01 mg/L experiment did not increase and is not included in this calculation. (Using the rate below, the 0.01 mg/L experiment would not see an increase in [Mn] of more than 0.08 nM (U.S. dust) and 0.015 nM (Saharan dust) over the first week, which is within the scatter of the duplicate measurements of both the control and the 0.01 mg/L experiment. Therefore, the low dust experiment does not constrain the initial rate.) The U.S. dust dissolution rate constant is 0.94 ± 0.04

$$\frac{nmol \; \text{Mn}}{day \cdot mg \; \text{Dust}},$$ and the Saharan dust dissolution rate constant is $0.22 \pm$ $0.01 \frac{nmol \; \text{Mn}}{day \cdot mg \; \text{Dust}}.$

4.1.2 Mn Thermodynamics

The Mn concentration versus time figures also show that dissolved Mn equilibrates between the dust and seawater after about two weeks. Each experimental treatment reaches a constant Mn concentration that is directly proportional to the dust concentration. The exception, 0.01 mg dust/L, had a final Mn concentration smaller than both the control and t=0 samples and was too similar to the control and t=0 samples throughout the experiment to distinguish any changes. It has not been considered in the following discussion. We also calculated the percentage of Mn dissolved from the dust using equation 4, where Mn_{dis} (defined as Mn passing through a 0.2 μm filter) is the dissolved plus colloidal Mn in solution, $[Mn]_{dust}$ is the Mn concentration in the dust (880 ppm for Saharan and 750 ppm for United States dust, taken from table 1), and [Dust] is the dust concentration,

$$\% Mn_{dis} = \frac{[Mn_{dis}]}{([Mn_{dust}][Dust])} \; . \qquad \text{(eq. 4)}$$

The seawater dissolved 12-14% of the total Mn from the Saharan dust, while the U.S. dust was slightly more soluble (17-20%, Fig. 5). These results, shown in figure 5, are lower but still comparable to previous studies which report Mn dissolution from a variety of dust particles in seawater from 25 – 30% (Chester et al., 1993; Guieu et al., 1994; Statham and Chester, 1988). Our results, in conjunction with previous work, lead to our determination that the final Mn concentration derived from dust dissolution is proportional to the dust concentration, but can be modeled using several different dissolution mechanisms.

4.1.3 Possible Mechanisms

We propose that Mn dissolution follows one of the following mechanisms. If we assume that all the manganese is adsorbed to the surface of the dust particles, then an adsorption –

desorption mechanism, where accessible Mn atoms can exchange with seawater cations, fits the data (Stumm and Morgan, 1996). In this simplification, all Mn within the dust is accessible. Although this is not absolutely correct, it will only differ from the true nature of the dust particles by a percentage of the total Mn. We have chosen to proceed with this simplification rather than apply an estimate of the percentage of Mn on the surface in order to stay as close to the unaltered natural dust as possible. In this reaction (eq. 5), using magnesium (Mg^{2+}) as an example, Mn acts as a tracer for cation exchange and is at a significantly lower concentration than Mg. Because of this large difference we assume that the magnesium concentration is unchanged during the adsorption process, and we are able to rewrite the equilibrium expression (eq. 6) to incorporate the magnesium terms in the chemical constant (eq. 7).

$$Mn(II) - dust + Mg^{2+} \underset{\longrightarrow}{\overset{\longleftarrow}{}} Mn^{2+} + Mg - dust \qquad \text{(eq. 5)}$$
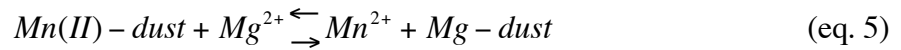
$$K^* = \frac{Mn^{2+}}{Mn - Dust} \frac{Mg - Dust}{Mg^{2+}} \qquad \text{(eq. 6)}$$

$$K = \frac{Mn^{2+}}{Mn - Dust} \qquad \text{(eq. 7)}$$

Figure 6 represents the total dissolved Mn against the total Mn bound to the dust (assuming that all Mn within the dust is accessible). The slope of the data in this figure is the apparent equilibrium constant, K, described by equation 7. The apparent constant is 0.21 ± 0.01 (nM Mn_{dis})/(nM Mn_{dust}) for the United States dust, and 0.16 ± 0.01 (nM Mn_{dis})/(nM Mn_{dust}) for the Saharan dust. In addition, the y-intercept of the experimental data is 0.93 ± 0.29 nM Mn for the United States dust, and 0.74 ± 0.29 nM for Saharan dust. As an additional test of the adsorption mechanism, these intercepts agree with our measured initial Mn_{dis} of 0.77 ± 0.10 nM Mn.

This type of reaction is driven by accessible surface sites on the dust which would allow for desorption of the Mn as well as adsorption in the reverse reaction. (Baker and Jickells, 2006) have shown that the surface area to volume ratio of mineral aerosol can be directly

proportional to the total leachable Fe from those aerosols. If Mn dissolution is solely driven by accessible Mn, then the dust with the greater surface area per mass should have the larger percent dissolution. We calculated the percentage of the total number of particles and the surface area per grain size for our dusts by using the percentage volume data from figure 2, assuming a density of 2.7 g/cm^3 and assuming spherical grains. The results of this calculation are presented in figure 7. From this calculation, the integrated surface area to volume ratio of the Saharan and US dusts are 0.93 μm^{-1} and 0.42 μm^{-1}, respectively. While these calculations are based on a greatly simplified dust particle shape and density, we believe that they can add substantive information to this mechanism. If the cation exchange reaction is surface area driven, then the Saharan dust would have a larger percent dissolution due to its larger surface area; however, the opposite is observed. Therefore we believe that the dissolution is driven by a mineral specific solubility rather than cation exchange, and that the total surface area of the dust particles is either not relevant to Mn dissolution or cannot be represented accurately through our simplified model.

The dissolution of a manganese mineral of the form Mn_xO_y, (where x = 1-2 and y = 1-3) could account for the observed data. Depending on the oxidation state of the Mn within the dust, we can describe the system in several different ways. The most common oxidation state found in terrestrial soils is Mn(II), which is highly soluble in water. If the dust contained Mn(II) minerals, the seawater would have dissolved all accessible Mn, leaving only Mn found deep within the matrix of the particles. In this scenario, the manganese minerals would have completely dissolved into the seawater in direct proportion to the amount of dust added. Although this is our observation, it is possible that part of the Mn within these dusts is of a higher oxidation state. Another explanation, which does not restrict the Mn to a 2+ oxidation state, can also account for the direct relationship between dust concentration and dissolved Mn. Mn(III) and Mn(IV) are insoluble in water and require reduction to the Mn(II) form in order to dissolve. This can be achieved by photoreduction of the oxidized Mn with organic material (Sunda *et al.*, 1983). Sunda *et al.*, (1983) demonstrated photochemical manganese oxide dissolution in seawater within Pyrex

bottles. The FEP Teflon bottles used in this experiment are 10-50% less transparent than Pyrex bottles in the visible wavelengths. However, they are more transparent in the UV, and photoreduction of manganese oxides is likely to occur. Once in solution, this later scenario is similar to the Mn^{2+} mechanism, and simply requires organic material to be present in order to keep the Mn^{2+} in the reduced and soluble form. The oxidation, or reoxidation in the cases of Mn(III) and Mn(IV), is prevented by the continued photoreduction of oxidized species back to Mn(II) and the very slow kinetics of oxidation (Stumm and Morgan, 1996). In this mechanism, the measured K_{eq} in figure 6 can be translated to an apparent solubility product.

The above mechanisms, reductive dissolution with Mn(II) mineral solubility or cation exchange, cannot be distinguished from each other given the data at hand. In addition, we could also be observing a combination of these reactions. If there was dissolution of Mn from a soluble mineral, Mn^{2+} could interact with surface adsorption sites following the adsorption – desorption process. These reactions, if they occurred on the same timescale, could each account for the observation of a chemical equilibrium and proportionality to total dust concentration.

An additional complication to the system is the presence of the Teflon wall. Although FEP will reduce metal adsorption, as compared to other plastics or glass, it will not completely eliminate the adsorption of Fe and Mn. This adsorption will remove Fe and Mn from the dissolved phase, and thus reduce our concentrations at each sub-sample. This process will reduce the calculated rates of dissolution of both Fe and Mn. In addition, the final concentrations will be reduced, and thus the apparent equilibrium constant measured will be a minimum estimate of the actual seawater constant.

4.2 Iron

4.2.1 Fe Kinetics

Dissolved Fe concentrations increase rapidly from an initial concentration of 0.165 ± 0.035 nM to ~ 0.6 nM (Fig. 1b). The rate of Fe dissolution was much faster than the rate of Mn dissolution and was also faster than our rate of sub-sampling. This is consistent with the reports of rapid kinetics for Fe complexation reactions (half-times of milliseconds to hours, (Rose and Waite, 2003)). In addition, [55]Fe uptake onto particulate and colloidal matter shows iron dissolution and adsorption occurring within seconds of dust addition (unpublished data, Guieu and Mendez). Because of our comparably slow sub-sampling, we cannot determine the initial dissolution rate for Fe. But given the initial increase of about 0.4 nM Fe between the time zero and the first sub-sampling (at 24 hours), we can determine that the initial dissolution rate is faster than 0.4 nM Fe/day (0.32 nmol Fe/day). Dissolved Fe remains mostly constant for the first week of the experiment, with only small increases up until day 7, where we see a second increase in Fe concentration between days 7 and 14 with little increase thereafter.

4.2.2 Fe Thermodynamics

The final Fe concentrations in these experiments are not dependent on dust concentration, and both Saharan and U.S. dusts yielded similar results. Indeed, nine of the ten samples (excluding the control) had a final iron concentration of 1.5 − 2.0 nM, the exception being the 5 mg/L U.S. dust experiment which fell within these values on day 14 and then increased to ~ 4 nM at the final sub-sampling day. Because of this consistency, we believe that Fe dissolution is a function of the seawater's individual dissolution capacity.

The dissolved Fe concentration in seawater is strongly affected by the thermodynamics of Fe solubility. The maximum solubility of amorphous iron hydroxides is 0.1 nM at the natural pH range of seawater (Morel and Hering, 1993). This limited dissolved iron concentration was reached before our experiment began; thus, there must be another mechanism for the observed increase in Fe solubility. It has long been believed that

seawater's Fe capacity is governed by the natural ligand complexing capacity within the water; we therefore propose that Fe dissolution is a function of the ligand concentration and the biological community, which are related to the source of the seawater.

This Fe dissolution mechanism is fundamentally different than the Mn dissolution mechanisms proposed above. Mn dissolution appears to follow a mechanism that is proportional to the source of Mn, while Fe does not. This difference in dissolution is driven by the large difference in solubility. While Mn(II) is highly soluble and seawater can dissolve as much Mn as is accessible from natural dust sources, Fe is very insoluble, and no matter how much dust is added, only a small total quantity of Fe may dissolve. Therefore, a large majority of the dissolved Fe must be associated with ligands in the seawater. The concentration of that ligand complexing capacity will dictate the solubility of Fe. We will refer to this possible Fe dissolution as the dust concentration independent mechanism.

4.2.3 Possible Mechanisms

The percentage of Fe dissolved from the dust is inversely proportional to both the concentration of dust and thus the mass of Fe within the dust. Using equation 8, we calculated the final percentage of Fe dissolved from the dust, (Fig. 8),

$$\% Fe_{dis} = \frac{[Fe_{dis}]}{([Fe_{dust}][Dust])} \quad , \qquad \text{(eq. 8)}$$

where $[Fe]_{dust}$ is 5.0% for Saharan and 3.8% for United States dust, taken from table 1. By holding $[Fe_{dis}]$ constant and only changing the dust concentration, we can model the proposed dust concentration independent model. The contours in figure 8 reflect Fe dissolution, which is independent of dust concentration. This dust concentration independent mechanism gives each line a slope of negative one (in log space) and is more sensitive to $[Fe_{dis}]$ changes at lower concentrations (due to the log-log scale). If dissolution is linearly proportional to dust concentration, the slope is zero, as demonstrated in the Mn

data in figure 5. Any slope between negative one and zero indicates a partial dependence on dust concentration.

The Saharan dust results (Fig. 8B) are consistent with the hypothesis that Fe dissolution is independent of dust concentration. The data have a slope of negative one and match the model at 1.5 nM (shown with a solid line). Also plotted on figure 8B is data from day 7 of Bonnet and Guieu, (2004) (the final day of their experiment) that used the same Saharan dust. Data from Bonnet and Guieu, (2004) are similar to our model; however, their data have a slope of -0.79 (± 3.7%) and therefore are partially dependent on dust concentration. The U.S. dust experiment (Fig. 8A) indicates that at the high dust concentrations there may be more Fe dissolution, similar to high dust concentration results in Bonnet and Guieu, (2004). However, the slope of the U.S. data is more consistent with the concentration independent mechanism suggested by the Saharan data (this study). Why should the same Saharan dust yield data reflecting different dissolution behavior? We believe that while the nature of the dust is important in controlling the mechanism of dissolution in seawater, the seawater itself is more important to the total dissolution. Therefore we must investigate the difference in the seawater used in these two experiments to understand the different behavior.

Total ligand measurements made aboard ship on seawater collected at the same depth and at nearly the same time of the water used for this experiment were:

$$[L_1]=1.67 \pm 0.03 \text{ nM} \quad \log K_1 = 12,$$

$$[L_2]=3.2 \pm 0.1 \text{ nM} \quad \log K_2 = 11. \quad \text{(Buck, K.N. pers. comm.)}$$

Adjusting for the relative strength of the L_2 ligand, the total Fe binding capacity of this water is 4.56 ± 0.10 nM. This indicates that the stoichiometry of the L_1 and L_2 ligands together to $[Fe]_{dis}$ is 3:1. The ligand measurements in this study give us an upper limit for ligand concentration and, therefore, Fe binding capacity. Our seawater was stored in the dark, but was not frozen between collection and the beginning of the experiment; therefore,

ligand concentrations most likely experienced thermochemical and photochemical decay. The ligand concentrations and their Fe binding capacity can only be used as a maximum. Despite this potential complication, the L_1 and L_2 concentrations measured at sea are close to the Fe concentration we measured in our experiments. This indicates that the ligand concentrations in the seawater are the primary controlling factors for Fe solubility, not the dust concentration. Bonnet and Guieu, (2004) examined the dissolution of anthropogenic particles showing extremely large dissolution of Fe, up to 13 nM. It is possible that this increase in solubility is due to an increase in labile iron associated with the anthropogenic particles as suggested by Bonnet and Guieu, (2004). This hypothesis is dependent upon on the availability of the iron atoms within the aerosol that would most likely be high in anthropogenic aerosols, which are typically composed of fine particles (Kiehl and Rodhe, 1995). A different yet complimentary hypothesis which can explain the increase in solubility is that the large organic component associated with typical anthropogenic aerosols (Heintzenberg, 1989) may act as weak Fe ligands. Under this hypothesis, the ligands which hold Fe in solution would simply come with the aerosol rather than being present in the seawater beforehand. A terrigenous particle, such as our Saharan and United States dusts, that did not undergo long range transport does not have as large an organic component as urban aerosol (Jacobson *et al.*, 2000), and thus a larger percentage of the ligands must originate from the biological community within the seawater.

Comparing the organic ligands between our seawater and the seawater used in Bonnet and Guieu, (2004) may elucidate reasons behind the difference between our results. Experimental conditions differed between the studies. Our study was held at 13°C under 50% of ambient light, whereas Bonnet and Guieu, (2004) conducted their experiments at 20°C under completely dark conditions. Bonnet and Guieu, (2004) may have found even higher dissolution if their experiment had been conducted with natural light due to photo-reduction of Fe to the soluble Fe^{2+} (Zhu *et al.*, 1993). The initial Fe concentration in our experiment's seawater was 0.165 ± 0.003 nM, which leads us to believe the measured

ligand concentrations are relatively small compared to those found in the Mediterranean. Ligand concentrations from the oligotrophic North Pacific have been measured at approximately 2 nM (Rue and Bruland, 1995), similar to the measured ligands in our study. However, in Bonnet and Guieu, (2004) the seawater had an initial Fe concentration of 0.38 nM, which may be due to a larger initial natural ligand concentration. Although the ligands were not measured in their experiment, ligand concentrations as high as 12 nM have been measured in the surface Western Mediterranean (van den Berg, 1995). These possible ligand concentrations could have increased the capacity of Fe in the water used in Bonnet and Guieu, (2004). This allowed more Fe to ultimately stay dissolved at the higher dust concentrations but does not explain the reason why the data indicate a partial dust concentration dependence.

5. Conclusions

Mn dissolution is dependent upon the dust concentration. This differs greatly from Fe dissolution due to the dramatic difference in Mn solubility compared to Fe. The exact mechanism for Mn dissolution from the dust particles cannot be determined from these experiments, but we are able to hypothesize that there is dissolution of Mn(II)-rich minerals which are held in the Mn (II) oxidation state through photo-reduction. Because of this, the type and quantity of dust is important and will affect both the kinetics and thermodynamics of Mn dissolution. We see that Saharan dust and U.S. dust react differently, and we believe this is due to the different mineral state of the Mn.

Fe dissolution is dependent on the water's ligand complexing capacity rather than the type or quantity of dust deposited on the surface. Dissolved inorganic Fe is saturated at 0.1 nM in natural seawater. Because of these thermodynamics, an increase in dust deposition will not increase Fe in the ocean, unless initial Fe inputs fertilize the ocean in such a way that the biologically community within the region is accustomed to dust deposition events and can produce ligands which will hold Fe in the dissolved form. Ultimately, the role of Fe

binding ligands toward atmospheric Fe dissolution is one of the important controls among the various processes controlling iron cycle in the surface waters.

TABLE

U.S. Dust	Saharan dust	Saharan end-member, Guieu *et al.*, 2002	Upper Crust, Wedepohl, 1995
Mn = 750 ppm	Mn = 880 ppm	-	Mn = 527 ppm
Fe = 3.81 %	Fe = 5.0%	Fe = 4.45 ± 0.49 %	Fe = 3.1 %
Al = 7.58 %	Al = 7.1 %	Al = 7.09 ± 0.49 %	Al = 7.7 %

Table 1: Elemental analysis of the dust samples used in the dissolution experiment. Measurements are total metal mass concentrations.

FIGURES
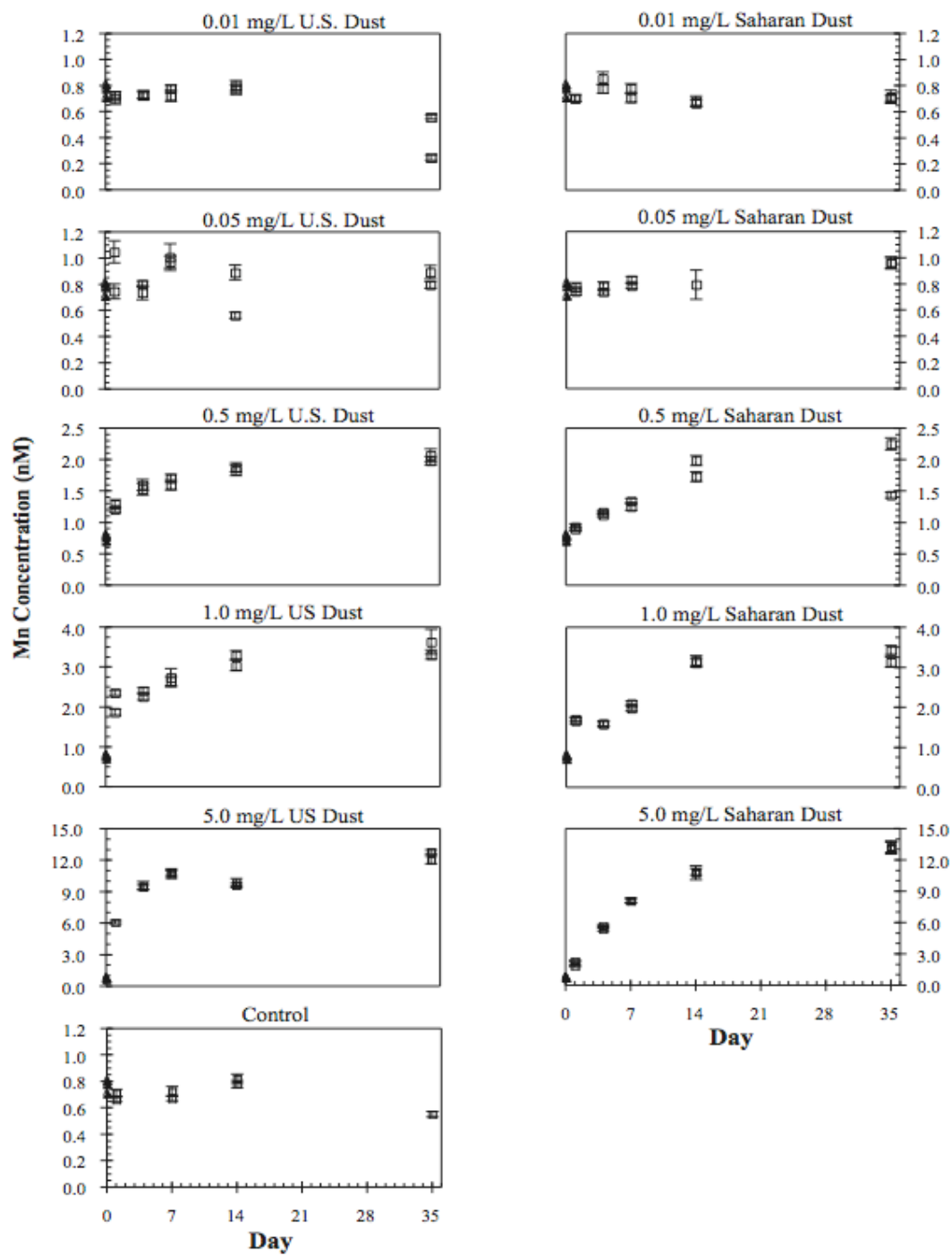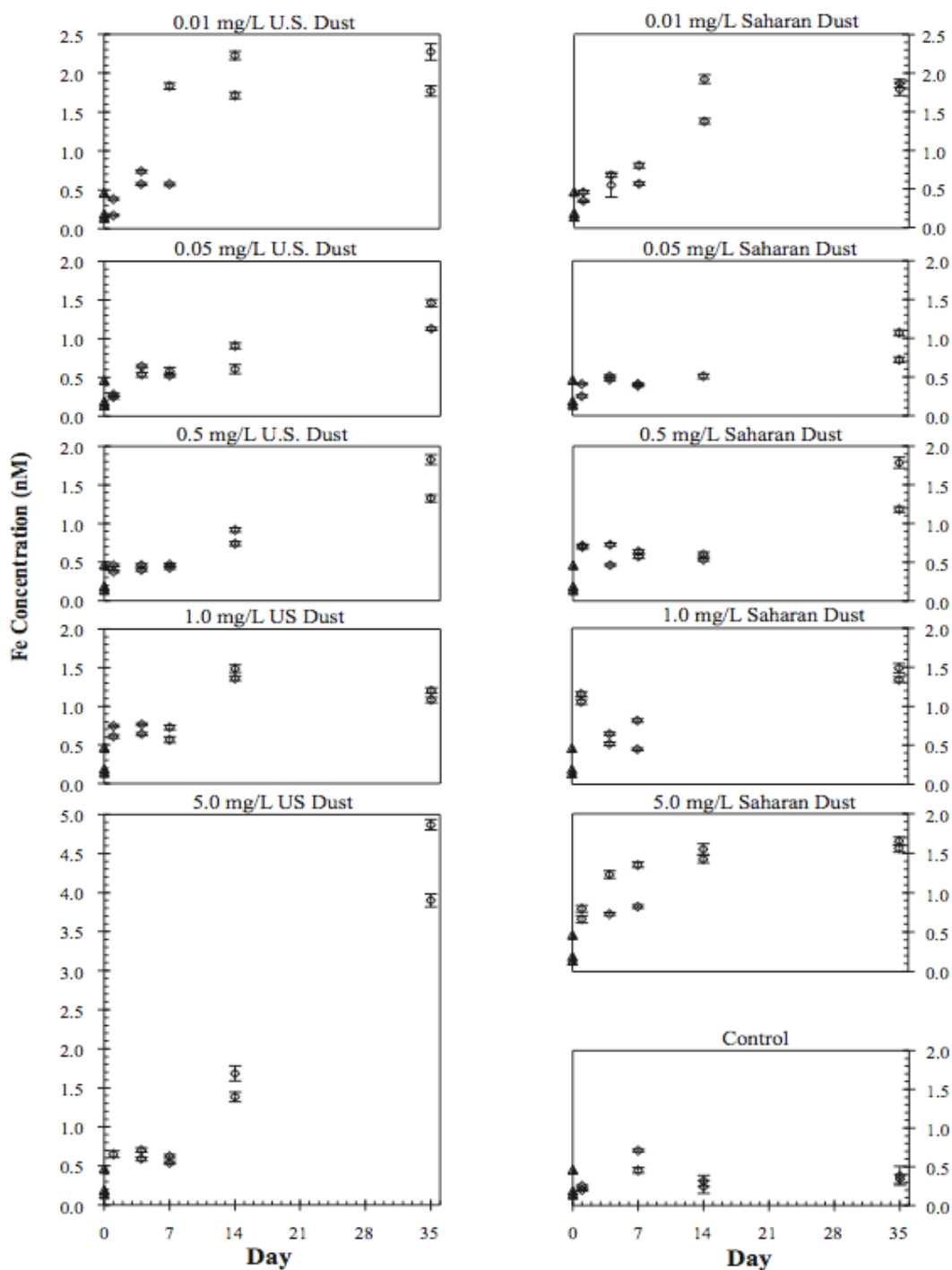
Figure 1: The concentration of (a) Mn versus time and (b) Fe versus time. Sub-samples (open squares, Mn; open diamonds, Fe) and the time zero samples (solid triangles) are plotted with 2 σ error bars.
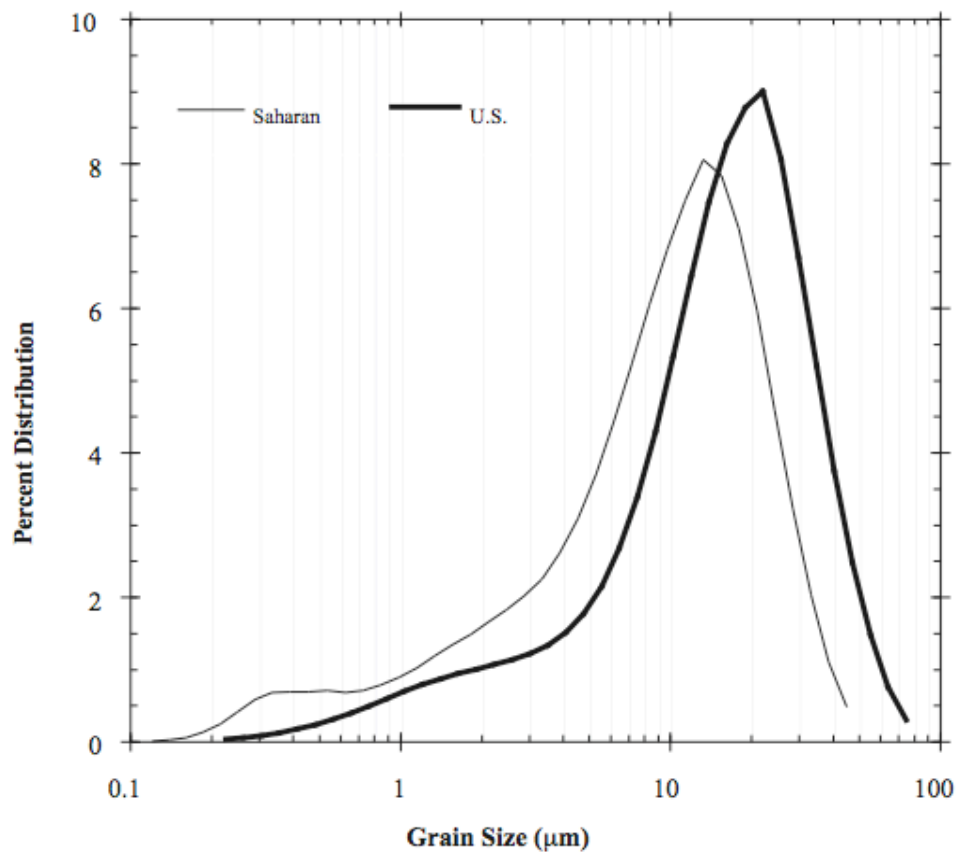
Figure 2: Size distribution of dust particles, in percentage of total volume. Saharan dust (thin line) has a group of particles below 0.6 μm, while this group is absent in the U.S. dust (heavy line).
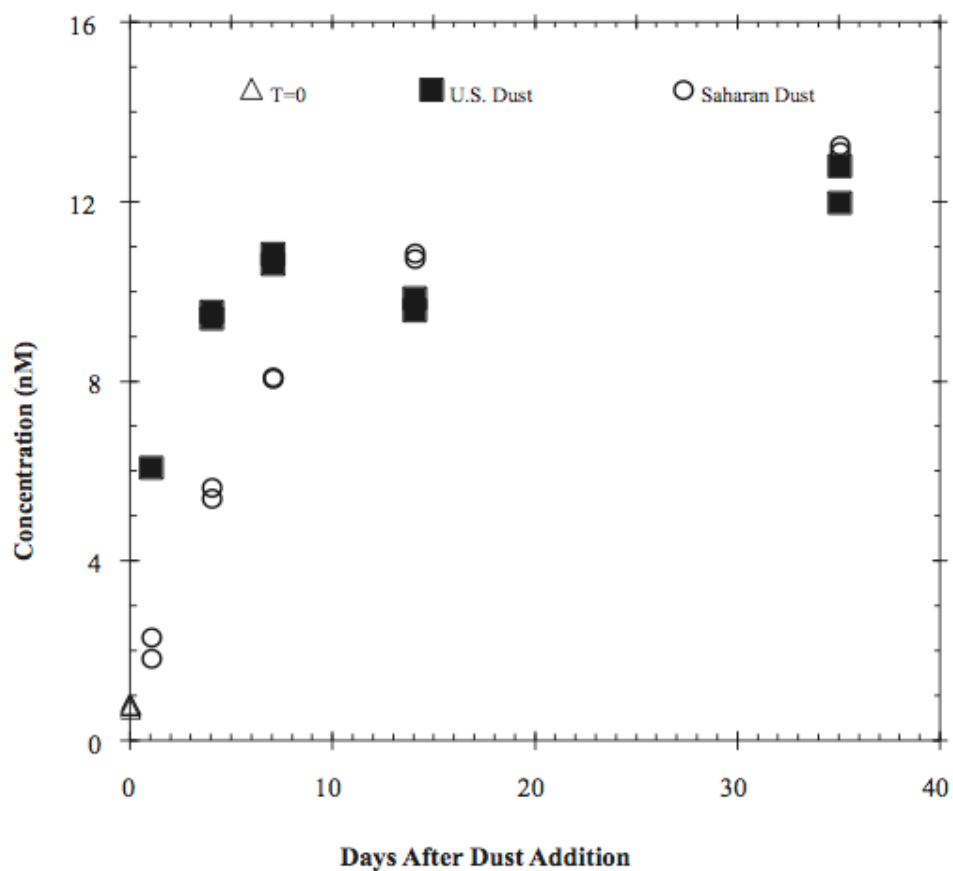
Figure 3: A comparison of Mn concentrations over time for the 5.0 mg/L of U.S. and Saharan dust samples. Mn concentrations before dust addition are represented by the open triangle, Saharan dust samples are represented by the closed square, and the U.S. dust is represented by the open circle. Error bars are 2 σ of the standard error.
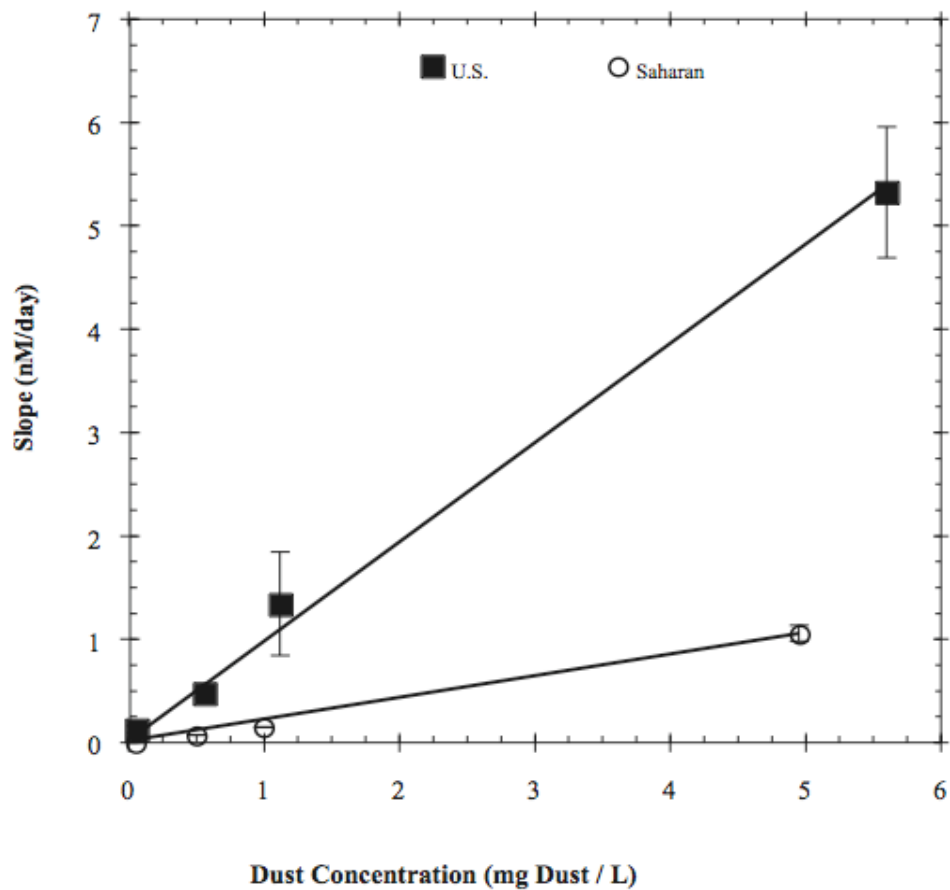
Figure 4: Plot of the slope of the initial increase in Mn concentration versus dust concentration. U.S. dust (closed squares) has a linear increase in slope with dust concentration which is an order of magnitude larger that the Saharan dust (open circles). Error bars are 2 σ of the standard error of the calculated slope.
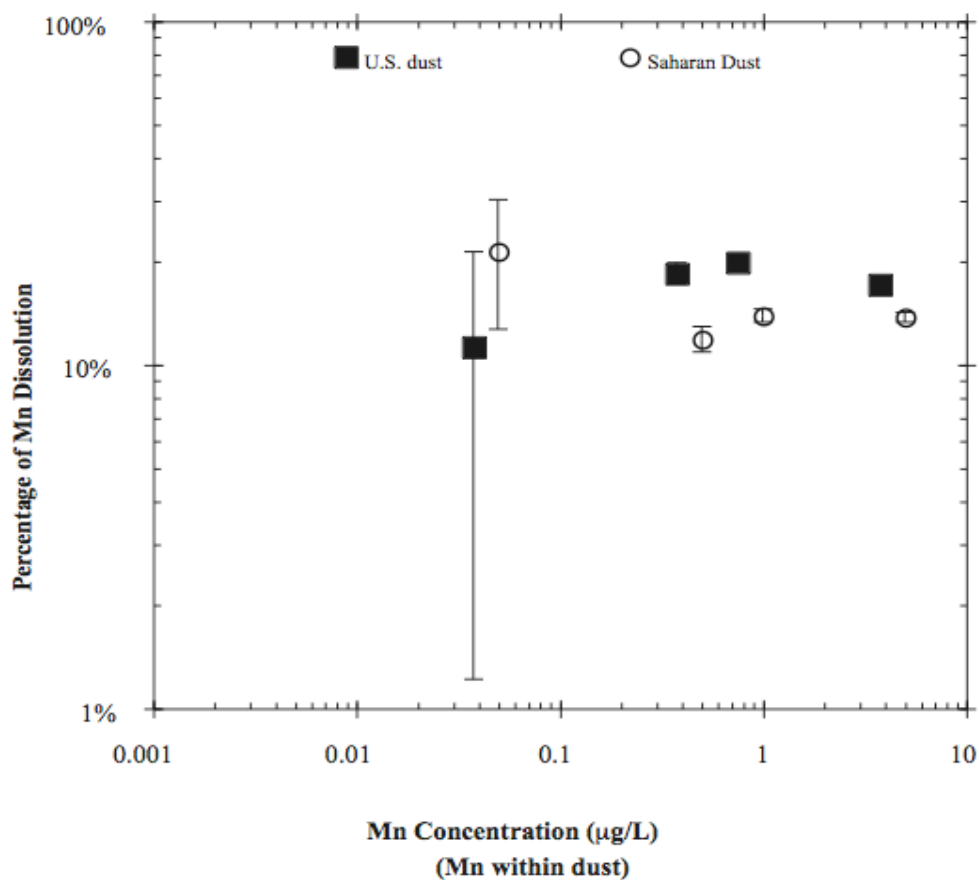
Figure 5: The percentage of Mn dissolved off the dust, taken on day 35 for the 4 highest dust concentrations. The error bars are 2 σ of the standard error of each individual sub-sample propagated through each step of the calculation, and averaged over the two duplicate sub-samples . The samples with low dust concentration have larger errors due to the relative small difference between the Mn increase over time and the initial Mn concentration. The log-log scale has been chosen in order to better compare with the analogous Fe plot, figure 8.
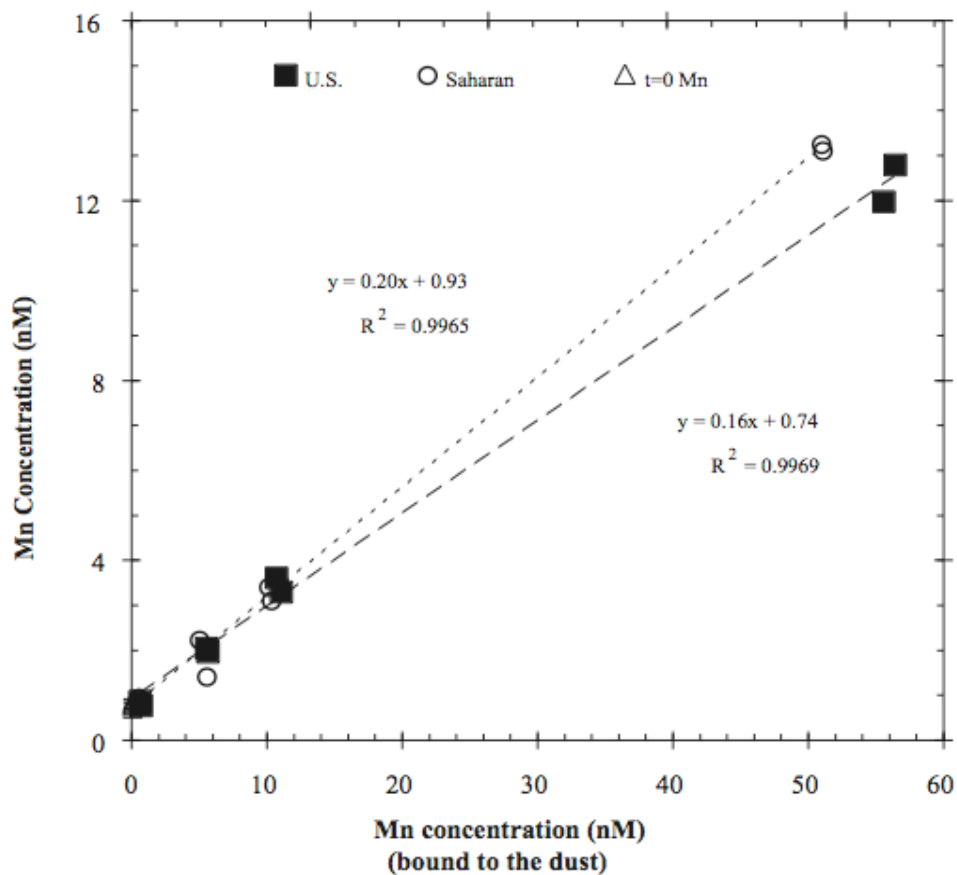
Figure 6: The Mn concentration (day 35) versus the total amount of Mn bound to the dust after dissolution. The Mn bound to the dust was calculated by subtracting the percent dissolved (equation 4) from 100% and multiplying that by the total concentration of Mn in the dust (using the data from table 1). The slope of the data will be the equilibrium constant described in the text.
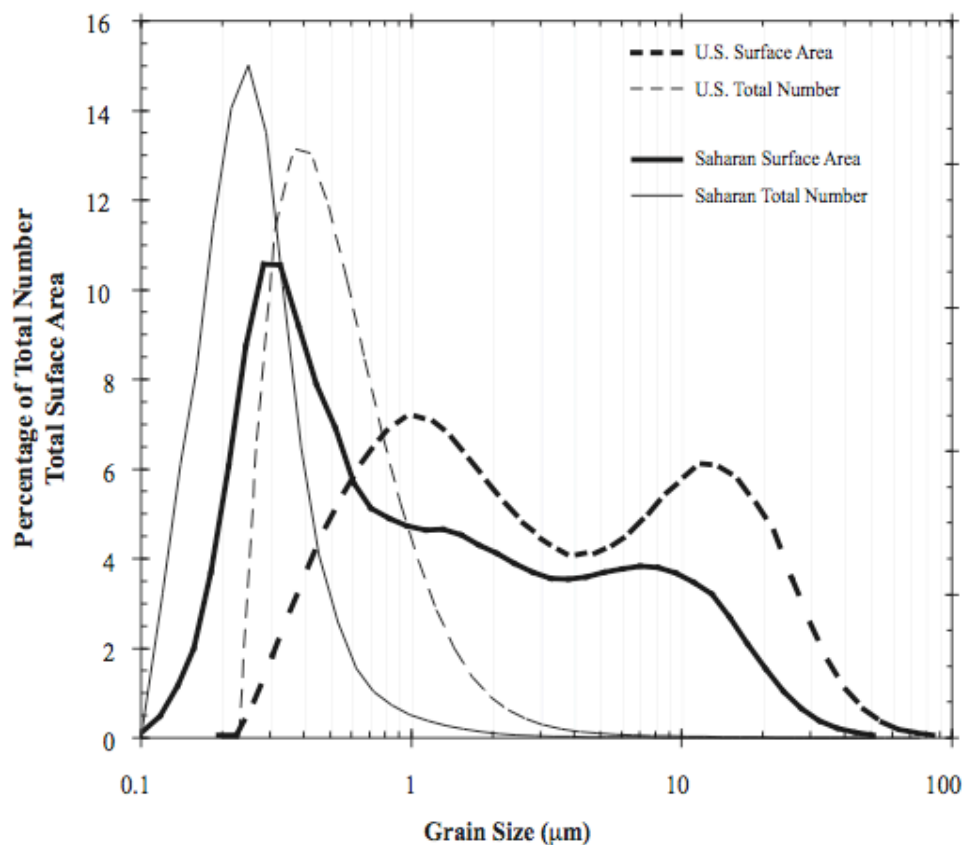
Figure 7: Percentage of surface area (heavy lines) and percentage of total particles number (thin lines) attributed to the size distribution of the dust particles. The Saharan dust (solid lines) has a large percentage of its surface area accounted for within the smaller sized particles, resulting in a larger surface area to volume ratio. The United States dust (dashed lines) has a particulate concentration at higher grain size, with a secondary group above 10 μm.
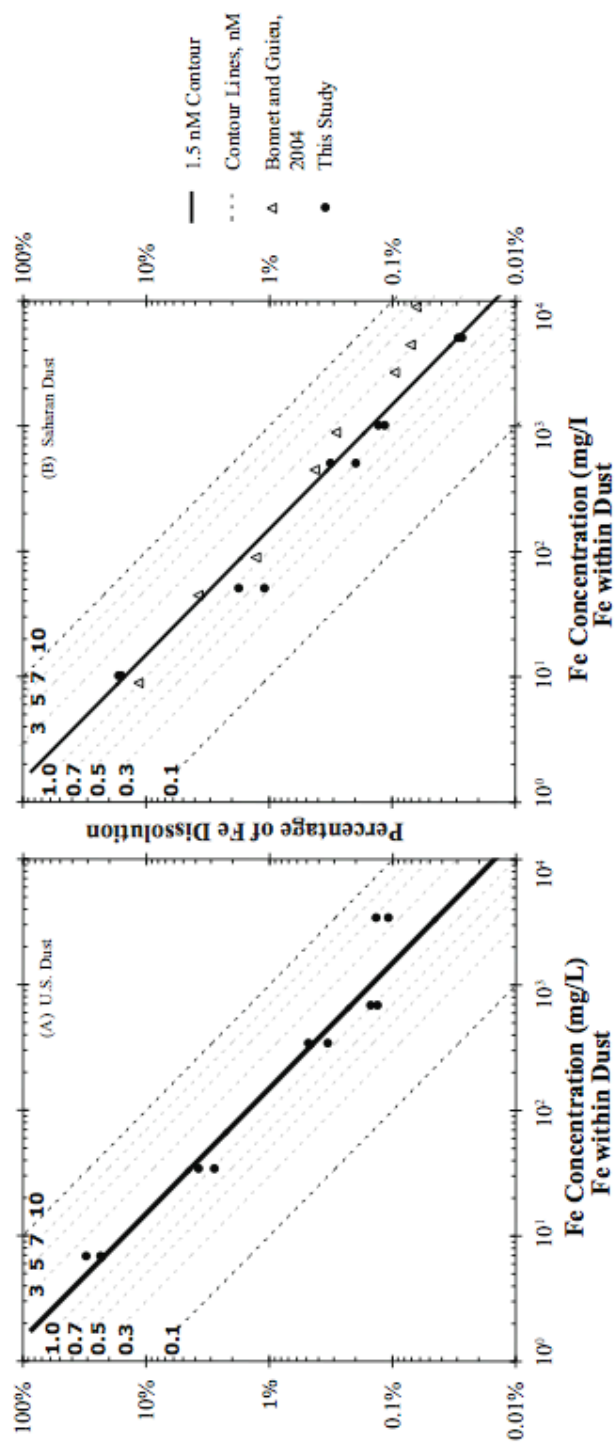
Figure 8: Percentage of Fe dissolved off of the dust after 35 days versus the total concentration of Fe introduced by the dust addition. (A) United States dust data (solid circles). (B) Saharan dust data (this study: solid circles) with data from Bonnet and Guieu, 2004 (open triangles) defined as dissolved Fe concentration in the experimental bottles. Both the Saharan dust and United States dust data are plotted on top of concentration contours from the dust concentration independent model (dashed and solid lines). Each contour represents the percentage of Fe dissolved from dust when the Fe concentration was held constant. Each line is labeled with the assumed constant Fe concentration (nM), both the U.S. and Saharan dust best fit the 1.5 nM line.

BIBLIOGRAPHY

Aumont, O., Maier-Reimer, E., Blain, S. and Monfray, P., 2003. An ecosystem model of the global ocean including Fe, Si, P colimitations. Global Biogeochemical Cycles, 17(2).

Baker, A.R. and Jickells, T.D., 2006. Mineral particle size as a control on aerosol iron solubility. Geophysical Research Letters, 33(L17608): 10.1029/2006GL026557.

Barbeau, K., 2006. Photochemistry of organic iron(III) complexing ligands in oceanic systems. Photochemistry and Photobiology, 82(6): 1505-1516.

Barbeau, K., Rue, E.L., Bruland, K.W. and Butler, A., 2001. Photochemical cycling of iron in the surface ocean mediated by microbial iron(III)-binding ligands. Nature, 413: 409-413.

Bonnet, S. and Guieu, C., 2004. Dissolution of atmospheric iron in seawater. Geophysical Research Letters, 31(3).

Buck, C.S., Landing, W.M., Resing, J.A. and Lebon, G.T., 2006. Aerosol iron and aluminum solubility in the northwest Pacific Ocean: Results from the 2002 IOC cruise. Geochemistry Geophysics Geosystems, 7.

Buck, K.N., M. C. Lohan, C. J. M. Berger, and K. W. Bruland 2007. Dissolved iron speciation in two distinct river plumes and an estuary: Implications for riverine iron supply. Limnology and Oceanography, 52(2).

Chester, R. et al., 1993. Factors Controlling the Solubilities of Trace-Metals from Nonremote Aerosols Deposited to the Sea-Surface by the Dry Deposition Mode. Marine Chemistry, 42(2): 107-126.

Duce, R.A. and Tindale, N.W., 1991. Atmospheric transport of iron and its deposition in the ocean. Limnology and Oceanography, 36(8): 1715-1726.

Gao, Y., Fan, S.M. and Sarmiento, J.L., 2003. Aeolian iron input to the ocean through precipitation scavenging: A modeling perspective and its implication for natural iron fertilization in the ocean. Journal of Geophysical Research-Atmospheres, 108(D7).

Guieu, C., Duce, R. and Arimoto, R., 1994. Dissolved Input of Manganese to the Ocean - Aerosol Source. Journal of Geophysical Research-Atmospheres, 99(D9): 18789-18800.

Guieu, C., Loye-Pilot, M.D., Ridame, C. and Thomas, C., 2002. Chemical characterization of the Saharan dust end-member: Some biogeochemical implications for the western Mediterranean Sea. Journal of Geophysical Research-Atmospheres, 107(D15).

Hand, J.L. et al., 2004. Estimates of atmospheric-processed soluble iron from observations and a global mineral aerosol model: Biogeochemical implications. Journal of Geophysical Research-Atmospheres, 109(D17).

Haygood, M.G., Holt, P.D. and Butler, A., 1993. Aerobactin Production by a Planktonic Marine Vibrio Sp. Limnology and Oceanography, 38(5): 1091-1097.

Heintzenberg, J., 1989. Fine particles in the global troposphere- a review. Tellus, 41B: 149-160.

Horsburgh, M.J., Wharton, S.J., Karavolos, M. and Foster, S.J., 2002. Manganese: elemental defense for a life with oxygen. Trends in Microbiology, 10(11): 496-501.

Jacobson, M.C., Hansson, H.C., Noone, K.J. and Charlson, R.J., 2000. Organic atmospheric aerosols: Review and state of the science. Reviews of Geophysics, 38(2): 267-294.

Kernen, N., Kidd, M.J., Penner-Hahn, J.E. and Pakrasi, H.B., 2002. A light-dependent mechanism for massive accumulation of manganese in the photosynthetic bacterium Synechocytis sp. PCC 6803. Biochemistry, 41(50): 15085-15092.

Kiehl, J.T. and Rodhe, H., 1995. Modeling geographical and seasonal forcing due to aerosols. Aerosol Forcing of Climate. Wiley, New York, 281-296 pp.

Klinkhammer, G.P. and Bender, M.L., 1980. The distribution of manganese in the Pacific Ocean. Earth and Planetary Science Letters, 46: 361-384.

Kraemer, S.M., Butler, A., Borer, P. and Cervini-Silva, J., 2005. Siderophores and the dissolution of iron-bearing minerals in marine systems, Molecular Geomicrobiology. Reviews in Mineralogy & Geochemistry, pp. 53-84.

Küpper, F.C., Carrano, C.J., Kuhn, J.U. and Butler, A., 2006. Photoreactivity of iron(III) - Aerobactin: Photoproduct structure and iron(III) coordination. Inorganic Chemistry, 45(15): 6028-6033.

Martin, J.H. and Fitzwater, S.E., 1988. Iron deficiency limits phytoplankton growth in the north-east Pacific subarctic. Nature, 331: 341-343.

Measures, C.I., Edmond, J.M. and Jickells, T.D., 1986. Aluminum in the Northwest Atlantic. Geochimica Et Cosmochimica Acta, 50(7): 1423-1429.

Moore, J.K., Doney, S.C., Lindsay, K., Mahowald, N. and Michaels, A.F., 2006. Nitrogen fixation amplifies the ocean biogeochemical response to decadal timescale variations in mineral dust deposition. Tellus Series B-Chemical and Physical Meteorology, 58(5): 560-572.

Morel, F.M.M. and Hering, J.G., 1993. Principles and Applications of Aquatic Chemistry. John Wiley & Sons, Inc., New york, 588 pp.

Nozaki, Y., Turekian, K.K. and Von Damm, D., 1980. 210Pb in GEOSECS water profiles from the North Pacific. Earth and Planetary Science Letters, 49: 393-400.

Rose, A.L. and Waite, T.D., 2003. Kinetics of iron complexation by dissolved natural organic matter in coastal waters. marine Chemistry, 84: 85-103.

Rue, E.L. and Bruland, K.W., 1995. Complexation of Iron(III) by Natural Organic-Ligands in the Central North Pacific as Determined by a New Competitive Ligand Equilibration Adsorptive Cathodic Stripping Voltammetric Method. Marine Chemistry, 50(1-4): 117-138.

Siefert, R.L., Johansen, A.M., Hoffmann, M.R. and Pehkonen, S.O., 1998. Measurements of trace metal (Fe, Cu, Mn, Cr) oxidation states in fog and stratus clouds. Journal of the Air & Waste Management Association, 48(2): 128-143.

Statham, P.J. and Chester, R., 1988. Dissolution of Manganese from Marine Atmospheric Particulates into Seawater and Rainwater. Geochimica Et Cosmochimica Acta, 52(10): 2433-2437.

Stumm, W. and Morgan, J.J., 1996. Aquatic Chemistry. Wiley-Interscience, New York, 1022 pp.

Sunda, W.G., Huntsman, S.A. and Harvey, G.R., 1983. Photoreduction of manganese oxides in seawater and its geochemical and biological implications. Nature, 301: 234-236.

Tegen, I. and Fung, I., 1994. Modeling of Mineral Dust in the Atmosphere - Sources, Transport, and Optical-Thickness. Journal of Geophysical Research-Atmospheres, 99(D11): 22897-22914.

van den Berg, C.M.G., 1995. Evidence for Organic Complexation of Iron in Seawater. Marine Chemistry, 50(1-4): 139-157.

Wu, J. and Boyle, E.A., 1997. Low Blank Preconcentration Technique for the Determination of Lead, Copper, and Cadmium in Small-Volume Seawater Samples by Isotope Dilution ICPMS. Analytical Chemistry, 69: 2464-2470.

Wu, J. and Boyle, E.A., 1998. Determination of iron in seawater by high-resolution isotope dilution inductively coupled plasma mass spectrometry after $Mg(OH)_2$ coprecipitation. Analytica Chimica Acta, 367: 183-191.

Zhu, X. et al., 1993. Photoreduction of Iron(Iii) in Marine Mineral Aerosol Solutions. Journal of Geophysical Research-Atmospheres, 98(D5): 9039-9046.